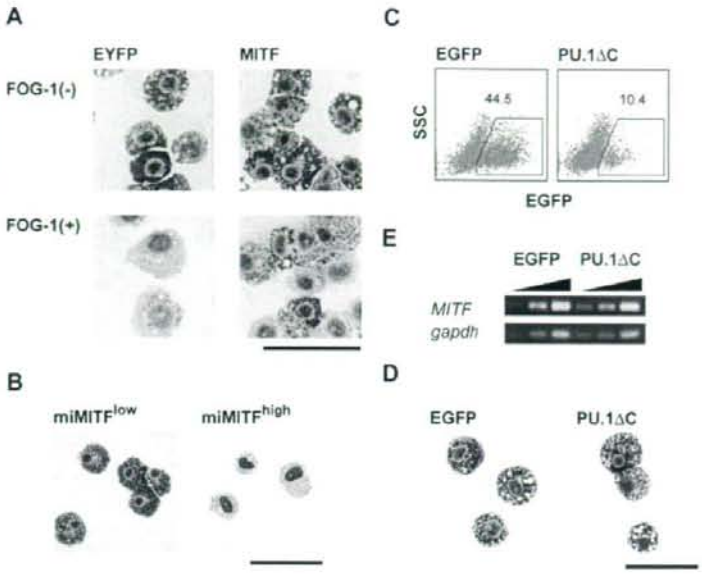

Figure 5. Requirement of *MITF* for mast cell–specific granule formation and the inhibition of the GATA-1: PU.1 interaction in mast cells. (A) Giemsa staining of EYFP$^+$ cells sorted 7 days after the infection of TET-FOG-1 mast cells with *LV-CAG-IRES-EYFP* (EYFP) and *LV-CAG-MITF-IRES-EYFP* (MITF). (B) Giemsa staining of *LV-CAG-miMITF-IRES-EYFP*-infected cells 7 days after infection. The *miMITF*-infected cells were sorted into 2 fractions, EYFP^{low} and EYFP^{high} (C-E). FACS analysis, Giemsa staining, and RT-PCR analysis of mast cells infected with *LV-CAG-IRES-EGFP* and *LV-CAG-PU.1ΔC-IRES-EGFP*. The cells were infected on day 21 and the analysis was carried out on day 28. RT-PCR was performed using the sorted EGFP$^+$ cells. Bars represent 50 μm.

(*FcεRβ*), *mast cell protease 4* (*p4*), *mast cell protease 5* (*p5*), *mast cell protease 6* (*p6*), *granzyme B* (*granB*), and *tryptophan hydroxylase* (*tph*) (Figure 4D), whereas that of *mast cell protease 1* (*p1*) and *carboxypeptidase A* (*cpa*) was not altered (Figure 4D). Consistent with our morphologic data, the changes in mRNA expression were reversed when *FOG-1* was no longer expressed (Figure 4E).

Effects of *MITF* on the phenotype of mast cells

Because *MITF* is crucial for mast-cell differentiation, down-regulation of *MITF* could cause the loss of mast-cell characteristics induced by *FOG-1*. Considering this, we analyzed the effects of *MITF* and its dominant-negative form (*miMITF*) on mast-cell granules. As shown in Figure 5A, the loss of mast-cell granules by *FOG-1* was rescued when *MITF* was coexpressed. To the contrary, *miMITF* induced the loss granules. Seven days after the introduction of *miMITF* into mature mast cells, the cells were sorted into 2 fractions, EYFP^{low} and EYFP^{high} (ie, high and low levels of MITF, respectively). Cytoplasmic basophilic granules were not detected in the EYFP^{high} mast cells (Figure 5B). To examine whether the rescue of *FOG-1*–mediated loss of granules by *MITF* was caused by direct functional antagonization and/or a direct interaction between FOG-1 and MITF, we carried out the following experiments. One is a reporter assay using MITF-responsible promoter for the analysis of functional antagonization. FOG-1 did not interfere with the MITF-driven transactivation (data not shown). The others are coimmunoprecipitation assay and yeast 2-hybrid assay for the direct association. However, no direct interaction was detected in the experiments (data not shown). These data suggest that the interference of MITF on FOG-1 function in this context is indirect.

Next, to exclude the possibility that the inhibitory effects of *FOG-1* on mast cell-specific gene expression were due to the abrogation of the association between PU.1 and the GATA factors, we carried out *PU.1ΔC* transduction into mast cells. A lentiviral vector was used because the retrovirus infection was not feasible for the infection to mast cells in our hands (data not shown). As shown in Figure 5C,D, *PU.1ΔC* did not affect mast-cell morphology. It is noteworthy that unlike *FOG-1*, *PU.1ΔC* did not down-regulate *MITF* expression (Figure 5E). Taken together, we conclude that the loss of basophilic granules caused by *FOG-1* was due to *MITF* down-regulation.

Discussion

In this study, we present the concept that the biologic function of *FOG-1* depends on its cellular context. From immature progenitors to mast cells, *FOG-1* preferentially induced neutrophilic differentiation. However, in mature mast cells, ectopic *FOG-1* expression resulted in a reversible loss of mast-cell features. We further showed that the context-dependent functions of *FOG-1* occur via distinct molecular mechanisms.

Lineage skewing to neutrophils caused by the disrupted association of GATA factors with PU.1

Overexpression of *FOG-1* at the progenitor stage decreased mast-cell differentiation and increased neutrophilic differentiation. These data suggest that neutrophilic expansion is caused by an alteration in cell fate from the mast-cell lineage to the neutrophilic lineage or by enhanced neutrophilic proliferation. If *FOG-1* induces extensive proliferation among neutrophilic progenitors and promotes mast cell death, the number of colonies should decrease, but the remaining colonies should contain a large number of neutrophils. However, the number of colonies was roughly comparable in the absence and presence of *FOG-1* (data not shown), and we did not observe hyperproliferative neutrophilic colonies. Together, these data suggest that *FOG-1* reprogrammed the fate of the cells from mast cells to neutrophils.

The next question involves the molecular mechanisms underlying the *FOG-1*–mediated lineage switch. In vitro differentiation using *GATA-1*–deficient ES cells showed that a loss of *GATA-1* causes neutrophilic expansion (Figure 2). Thus, we entertained the idea that FOG-1 inhibited the function of GATA-1 by abrogating

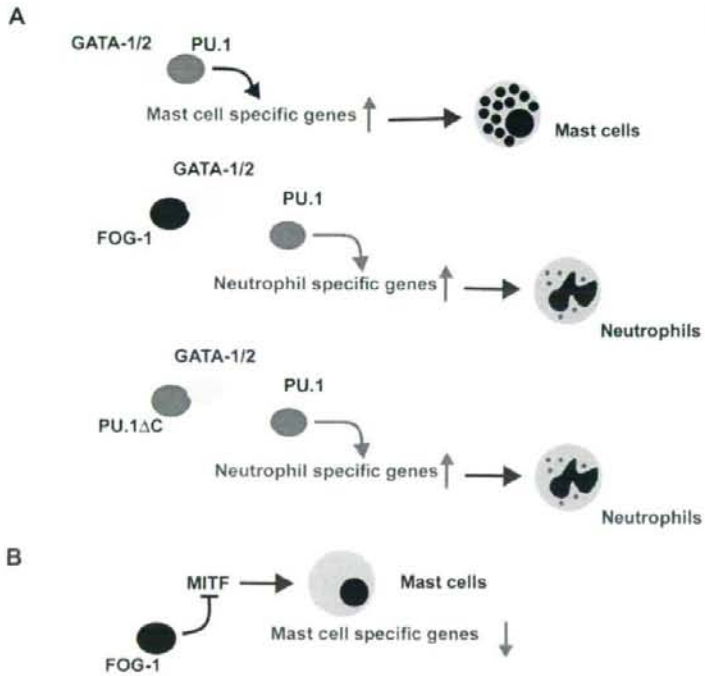

Figure 6. Cell context-dependent function of FOG-1. (A) Schematic model of the lineage switch from mast-cells to neutrophils by *FOG-1* and *PU.1ΔC*. (B) The down-regulation of mast cell specific gene expression by *FOG-1* expression in mature mast cells.

the interaction between GATA factors and PU.1. *PU.1* was originally identified as a candidate oncogene for erythroleukemia,[29] and it has been shown that PU.1 physically interacts with GATA-1 and GATA-2.[30] Although PU.1 antagonizes GATA-1 in erythroid cells, cooperation between GATA-2 and PU.1 has been demonstrated during mast-cell differentiation.[26] Thus, we hypothesized that the molecular and functional interactions between GATA-1 and PU.1 would be influenced by FOG-1 during mast-cell differentiation. Immunoprecipitation assays revealed that GATA-1 and PU.1 complex formation was disrupted by FOG-1.

Meanwhile, during erythropoiesis, PU.1 blocks GATA-1–mediated erythroid maturation[31] and it has been shown that PU.1 creates a repressive chromatin conformation by binding to GATA-1 on several erythroid-specific gene promoters.[32] It is thus conceivable that FOG-1 relieves the PU.1-mediated suppression of GATA-1 during erythropoiesis. Likewise, the reduction in GATA factor/PU.1 binding by FOG-1 would inhibit mast-cell differentiation (Figure 6A). Our data using PU.1ΔC strongly support this idea.

The erythro/megakaryocytic and mast-cell lineages share several transcription factors, including *GATA-1*, *GATA-2*, and *SCL*. The expression patterns of these factors raise the question of whether mast cells should be categorized within the erythro/megakaryocyte compartment. Our data demonstrate that *FOG-1* overexpression at the mast-cell progenitor stage favors the development of neutrophils. This suggests a similarity between mast cells and neutrophils. It is noteworthy that it has been shown that mast-cell progenitors are derived from granulocyte/monocyte progenitors (GMP) via bipotent basophil/mast cell progenitors (BMCP) and also that megakaryocyte/erythrocyte progenitors (MEP) do not differentiate into mast cells under the same conditions.[33]

However, in *FOG-1*-null and *GATA-1^{low}* mice, unusual trilineage colonies containing erythroid, megakaryocytes, and mast-cells have been observed in vivo.[9,14] This raises the possibility that mast cells and erythroid/megakaryocytic cells are derived from a common progenitor, but *GATA-1*-deficient proerythroblastic cells can be trans-differentiated into mast cells by IL-3 stimulation.[34] Thus, the trilineage progenitors may stem from trans-differentiation of erythroid/megakaryocytic cells via a loss of complex formation between GATA-1 and FOG-1. Taken together, it is reasonable to consider that mast cells are close to the macrophage/neutrophil lineage under physiologic conditions, and a lack of GATA-1/FOG-1 complex formation produces changes in the erythroid-megakaryocytic compartment that enable mast-cell differentiation.

Loss of the mast cell phenotype by down-regulation of *MITF*

FOG-1 reduced mast cell–specific gene expression in mature mast cells (Figure 4D). Because this effect was reversible (Figure 4E), *FOG-1* must inhibit transcriptional machinery that is continuously necessary for the trans-activation of mast cell–specific genes. GATA-1 and PU.1 synergistically activate several mast cell–specific promoters; however, the loss of mast-cell granules by FOG-1 was not caused by interruption of the complex between the GATA factors and PU.1 because the overexpression of PU.1ΔC did not influence the morphology of the mast cells.

MITF, a critical transcriptional regulator of mast-cell differentiation, was significantly down-regulated by *FOG-1*. *MITF* hypomorphic mutant (*mi/mi*) mice have reduced numbers of differentiated mast cells,[35,36] whereas the mast cells present in the skin of *mi/mi* mice lack *p4* and *p5*, but not *cpa* mRNA.[37,38] Thus, *MITF* is critical for the development and differentiation of mast cells, as well as for the expression of lineage-specific genes responsible for their physiologic functions. When *FOG-1* is expressed in mast cells,

mRNA expression of *p4* and *p5* is reduced, whereas that of *cpa* is unaffected. The change in mRNA expression by *FOG-1* was very similar to that in *mi/mi* mast cells and to that induced by *miMITF* expression in differentiated ES cell–derived mast cells in vitro (data not shown). Furthermore, the effects of *FOG-1* on mast cells were reversed by the overexpression of wild-type *MITF*. Overall, the alterations in mast-cell phenotype caused by *FOG-1* can be explained by the down-regulation of *MITF*, which is quite different from the molecular mechanism involved in lineage skewing (ie, reduced complex formation between the GATA factors and PU.1) (Figure 6). One role of *FOG-1* in erythroid and megakaryocytic differentiation may be the inactivation of mast cell–specific gene expression through the repression of *MITF*.

Differential context dependent effects of *FOG-1* during mast-cell differentiation

Our previous studies using an OP9 in vitro hematopoietic differentiation induction system revealed that the biologic functions of hematopoietic transcription factors and cofactors depend on the context of differentiation. By combining this system with a tetracycline-based gene-expression system in *GATA-1*–deficient ES cells, we found that the role of *GATA-1* during erythropoiesis is differentiation stage–dependent.[22] We also found 2 context-dependent functions of *GATA-2* during cell differentiation.[21] First the lineage-redirecting ability of *GATA-2* is influenced by the timing of the *GATA-2* expression, and second, GATA-2 and a fusion protein between GATA-2 and the estrogen receptor ligand binding domain have opposite effects on the proliferation of hematopoietic progenitors. These findings suggest that the context-dependent effects of GATA-2 and GATA-1 result from the particular proteins with which these factors interact.

The biologic function of *FOG-1* during erythropoiesis and megakaryopoiesis also depends on the cell context. *FOG-1* inhibited cellular proliferation in early immature megakaryocytes, but it enhanced cellular proliferation and disrupted cellular maturation in late megakaryocytic cells.[20] Thus, transcription factors and cofactors can produce different biologic effects on lineage commitment, cell proliferation, and maturation in hematopoietic cells depending on the differentiation status of the cells. To clarify the role of hematopoietic transcription factors and cofactors during hematopoiesis, it will be necessary to analyze gain- and loss-of-function mutants in lineage- and stage-defined hematopoietic cells. In vitro hematopoietic differentiation in ES cells using the OP9 system will be a useful tool for understanding the context-dependent biologic functions of transcription factors and cofactors.

Acknowledgments

We thank Drs T. Kitamura, K. Ohishi, T. Oikawa, H. Karasuyama, E. Morii, M. Yamamoto, M. Ikawa, S. H. Orkin, and Amgen (Thousand Oaks, CA) for providing materials. We also thank Ms A. Mizokami for her assistance.

This work was supported in part by Grants-in-Aid for Scientific Research from the Ministry of Education, Culture, Sports, Science and Technology (MEXT), and Osaka University 21st Century COE program "CICET," Japan.

Authorship

Contribution: D.S., M.T., K.K., J.Z., and H.Y. performed research on both molecular and cell biology. T.M. and A.Y. carried out the analysis of histamine release. T.N. designed this research and wrote the manuscript.

Conflict-of-interest disclosure: The authors declare no competing financial interests.

Correspondence: Toru Nakano, Department of Stem Cell Pathology, Medical School, Osaka University, 2-2 Yamada-oka, Suita, Osaka 565-0871, Japan; e-mail: tnakano@patho.med.osaka-u.ac.jp.

References

1. Metcalf D. On hematopoietic stem cell fate. Immunity. 2007;26:669-673.
2. Orkin SHGAT A-binding transcription factors in hematopoietic cells. Blood. 1992;80:575-581.
3. Martin DI, Zon LI, Mutter G, Orkin SH. Expression of an erythroid transcription factor in megakaryocytic and mast cell lineages. Nature. 1990;344:444-447.
4. Zon LI, Yamaguchi Y, Yee K, et al. Expression of mRNA for the GATA-binding proteins in human eosinophils and basophils: potential role in gene transcription. Blood. 1993;81:3234-3241.
5. Pevny L, Simon MC, Robertson E, et al. Erythroid differentiation in chimaeric mice blocked by a targeted mutation in the gene for transcription factor GATA-1. Nature. 1991;349:257-260.
6. Weiss MJ, Keller G, Orkin SH. Novel insights into erythroid development revealed through in vitro differentiation of GATA-1 embryonic stem cells. Genes Dev. 1994;8:1184-1197.
7. Fujiwara Y, Browne CP, Cunniff K, Goff SC, Orkin SH. Arrested development of embryonic red cell precursors in mouse embryos lacking transcription factor GATA-1. Proc Natl Acad Sci U S A. 1996;93:12355-12358.
8. Shivdasani RA, Fujiwara Y, McDevitt MA, Orkin SH. A lineage-selective knockout establishes the critical role of transcription factor GATA-1 in megakaryocyte growth and platelet development. EMBO J. 1997;16:3965-3973.
9. Migliaccio AR, Rana RA, Sanchez M, et al. GATA-1 as a regulator of mast cell differentiation revealed by the phenotype of the GATA-1low mouse mutant. J Exp Med. 2003;197:281-296.
10. Tsai FY, Orkin SH. Transcription factor GATA-2 is required for proliferation/survival of early hematopoietic cells and mast cell formation, but not for erythroid and myeloid terminal differentiation. Blood. 1997;89:3636-3643.
11. Tsang AP, Visvader JE, Turner CA, et al. FOG, a multitype zinc finger protein, acts as a cofactor for transcription factor GATA-1 in erythroid and megakaryocytic differentiation. Cell. 1997;90:109-119.
12. Chang AN, Cantor AB, Fujiwara Y, et al. GATA-factor dependence of the multitype zinc-finger protein FOG-1 for its essential role in megakaryopoiesis. Proc Natl Acad Sci U S A. 2002;99:9237-9242.
13. Shimizu R, Ohneda K, Engel JD, Trainor CD, Yamamoto M. Transgenic rescue of GATA-1-deficient mice with GATA-1 lacking a FOG-1 association site phenocopies patients with X-linked thrombocytopenia. Blood. 2004;103:2560-2567.
14. Tsang AP, Fujiwara Y, Hom DB, Orkin SH. Failure of megakaryopoiesis and arrested erythropoiesis in mice lacking the GATA-1 transcriptional cofactor FOG. Genes Dev. 1998;12:1176-1188.
15. Wang X, Crispino JD, Letting DL, Nakazawa M, Poncz M, Blobel GA. Control of megakaryocyte-specific gene expression by GATA-1 and FOG-1: role of Ets transcription factors. EMBO J. 2002;21:5225-5234.
16. Letting DL, Chen YY, Rakowski C, Reedy S, Blobel GA. Context-dependent regulation of GATA-1 by friend of GATA-1. Proc Natl Acad Sci U S A. 2004;101:476-481.
17. Pal S, Cantor AB, Johnson KD, et al. Coregulator-dependent facilitation of chromatin occupancy by GATA-1. Proc Natl Acad Sci U S A. 2004;101:980-985.
18. Era T, Witte ON. Regulated expression of P210 Bcr-Abl during embryonic stem cell differentiation stimulates multipotential progenitor expansion and myeloid cell fate. Proc Natl Acad Sci U S A. 2000;97:1737-1742.
19. Kitajima K, Masuhara M, Era T, Enver T, Nakano T. GATA-2 and GATA-2/ER display opposing activities in the development and differentiation of blood progenitors. EMBO J. 2002;21:3060-3069.
20. Tanaka M, Zheng J, Kitajima K, Kita K, Yoshikawa H, Nakano T. Differentiation status dependent function of FOG-1. Genes Cells. 2004;9:1213-1226.
21. Kitajima K, Tanaka M, Zheng J, et al. Redirecting differentiation of hematopoietic progenitors by a transcription factor, GATA-2. Blood. 2006;107:1857-1863.
22. Zheng J, Kitajima K, Sakai E, et al. Differential effects of GATA-1 on proliferation and differentiation of erythroid lineage cells. Blood. 2006;107:520-527.
23. Morita S, Kojima T, Kitamura T. Plat-E: an efficient and stable system for transient packaging of retroviruses. Gene Ther. 2000;7:1063-1066.

24. Yamamoto H, Kihara-Negishi F, Yamada T, Hashimoto Y, Oikawa T. Physical and functional interactions between the transcription factor PU. 1 and the coactivator CBP. Oncogene. 1999;18: 1495-1501.
25. Zon LI, Gurish MF, Stevens RL, et al. GATA-binding transcription factors in mast cells regulate the promoter of the mast cell carboxypeptidase A gene. J Biol Chem. 1991;266:22948-22953.
26. Walsh JC, DeKoter RP, Lee HJ, et al. Cooperative and antagonistic interplay between PU. 1 and GATA-2 in the specification of myeloid cell fates. Immunity. 2002;17:665-676.
27. Nerlov C, Graf T. PU. 1 induces myeloid lineage commitment in multipotent hematopoietic progenitors. Genes Dev. 1998;12:2403-2412.
28. Nerlov C, Querfurth E, Kulessa H, Graf T. GATA-1 interacts with the myeloid PU. 1 transcription factor and represses PU. 1-dependent transcription. Blood. 2000;95:2543-2551.
29. Fisher RC, Scott EW. Role of PU. 1 in hematopoiesis. Stem Cells. 1998;16:25-37.
30. Zhang P, Behre G, Pan J, et al. Negative cross-talk between hematopoietic regulators: GATA proteins repress PU. 1. Proc Natl Acad Sci U S A. 1999;96:8705-8710.
31. Zhang P, Zhang X, Iwama A, et al. PU. 1 inhibits GATA-1 function and erythroid differentiation by blocking GATA-1 DNA binding. Blood. 2000;96: 2641-2648.
32. Stopka T, Amanatullah DF, Papetti M, Skoultchi AI. PU. 1 inhibits the erythroid program by binding to GATA-1 on DNA and creating a repressive chromatin structure. EMBO J. 2005;24:3712-3723.
33. Arinobu Y, Iwasaki H, Gurish MF, et al. Developmental checkpoints of the basophil/mast cell lineages in adult murine hematopoiesis. Proc Natl Acad Sci U S A. 2005;102:18105-18110.
34. Kitajima K, Zheng J, Yen H, Sugiyama D, Nakano T. Multipotential differentiation ability of GATA-1-null erythroid-committed cells. Genes Dev. 2006; 20:654-659.
35. Takebayashi K, Chida K, Tsukamoto I, et al. The recessive phenotype displayed by a dominant negative microphthalmia-associated transcription factor mutant is a result of impaired nucleation potential. Mol Cell Biol. 1996;16:1203-1211.
36. Kataoka TR, Morii E, Oboki K, Jippo T, Maeyama K, Kitamura Y. Dual abnormal effects of mutant MITF encoded by Mi(wh) allele on mouse mast-cells: decreased but recognizable transactivation and inhibition of transactivation. Biochem Biophys Res Commun. 2002;297:111-115.
37. Morii E, Tsujimura T, Jippo T, et al. Regulation of mouse mast cell protease 6 gene expression by transcription factor encoded by the mi locus. Blood. 1996;88:2488-2494.
38. Morii E, Jippo T, Tsujimura T, et al. Abnormal expression of mouse mast cell protease 5 gene in cultured mast cells derived from mutant mi/mi mice. Blood. 1997;90:3057-3066.

Arch Histol Cytol, 71 (1): 37-44 (2008)

The modulation of collagen fibril assembly and its structure by decorin: An electron microscopic study*

Shunsuke Iwasaki[1], Yoshinao Hosaka[1], Tomohito Iwasaki[2], Katsuhiro Yamamoto[2], Aya Nagayasu[1], Hiromi Ueda[1], Yasuo Kokai[3], and Kazushige Takehana[1]

[1]Department of Veterinary Anatomy, School of Veterinary Medicine, and [2]Department of Applied Biochemistry, School of Dairy Science, Rakuno Gakuen University, Ebetsu; and [3]Department of Biomedical Engineering, School of Medicine, Sapporo Medical University, Sapporo, Japan

Summary. The present study was carried out to determine the effect of decorin in the process of collagen assembly. Collagen fibrils were obtained *in vitro* by aggregation from commercialized acid-soluble type I collagen with the addition of different concentrations of decorin (0–25 μg/ml). All specimens were observed by scanning electron microscopy (SEM) and transmission electron microscopy (TEM). The distribution of collagen fibril diameters was also analyzed by TEM. In samples without or with low concentrations of decorin, highly porous collagen fiber networks were formed. On the other hand, dense networks were observed in samples treated with high concentrations of decorin. The influence of decorin secreted by cells on collagen fibrils was observed by SEM, and the fiber network elasticity was measured using a rheometer. SEM images showed that collagen fiber networks without fibroblasts were much looser than those cultured with normal fibroblasts. The networks cultured with the fibroblasts were composed of straight fibers with large diameters. On the other hand, collagen fiber networks cultured with siRNA-decorin-transfected (siDT) fibroblasts had loose, meandering fibers with small diameters. The elasticity of collagen fiber networks cultured with untransfected fibroblasts showed no significant difference over the 7-day incubation period. However, significantly lower elastic values were obtained for collagen fiber networks treated with siDT cells on days 3 and 7. In addition, after treatment with 5.0 or 25 μg/ml decorin, the collagen fiber networks cultured with siDT cells exhibited an altered structure that showed a dense structure similar to that of the fiber networks cultured with untransfected fibroblasts. In conclusion, this *in vitro* study showed that decorin is a regulatory and architecturally small leucine-rich repeat proteoglycan in the process of collagen fibril assembly.

Received November 20, 2007; revised March 7, 2008

* This study was supported in part by a Grant-in Aid for Scientific Research from Ministry of Education, Sports and Culture, Japan to Y.H. (No. 19780220) and by a grant from the Akiyama Foundation, Japan to Y.H. (No. 200518).

Address for correspondence: Dr. Yoshinao Hosaka, Department of Veterinary Anatomy, Faculty of Agriculture, Tottori University, 4-101 Koyama-Minami, Tottori 680-8553, Japan
Tel and Fax: +81-857-31-5572
E-mail:y-hosa@muses.tottori-u.ac.jp

Introduction

Connective tissues, such as the dermis, bone, tendons and ligaments, are primarily composed of collagen fibers, which are formed by type I collagen. There are also various non-collagenous proteins — proteoglycans (PGs), and glycosaminoglycans (GAGs) — which interact with the fibrillar collagen network. Many studies have suggested that interactions between collagens, PGs, and/or GAGs play an important role in the process of collagen fibrogenesis and assembly.

Decorin, a small leucine-rich repeat PG (SLRP), is expressed by a variety of cells, including fibroblasts, myocytes, and smooth muscle cells (Thieszen and

Roesenquist, 1995; Hocking *et al.*, 1998, Nishimura *et al.*, 2003). In connective tissue, it is thought that decorin participates in the regulation of collagen fibrogenesis by binding collagen fibrils (Bidanset *et al.*, 1992; Kresse *et al.*, 1997; Iozzo *et al.*, 1999) in cooperation with other SLRPs and a variety of growth factors (Yamaguchi *et al.*, 1990; Hildebrand *et al.*, 1994; Grinnell *et al.*, 2000; Hosaka *et al.*, 2005). Sini *et al.* (1997) performed a morphological study that showed the role of decorin in the *in vitro* fibrogenesis of type I collagen and concluded that decorin exerted different effects on phases of fibril formation in correlation with the degree of glycosylation of the collagen. Therefore, decorin might influence the assembly and diameter of collagen fibrils by binding to their surfaces.

Several independent studies using materials such as chicken embryos and mouse tendons have suggested that decorin delays individual collagen molecule fusion (Vogel *et al.*, 1984; Vogel and Trotter, 1987; Birk *et al.*, 1995, 1996). It has also been shown that decorin determines the interfibrillar space of collagen fibrils by regulating the length of side chains (Kuwaba *et al.*, 2001, 2002; Watanabe *et al.*, 2005, 2007). Decorin also acts as an intermediary between type I collagen and some types of collagen (Nareyeck *et al.*, 2004).

Gene-targeting studies using decorin-deficient mice have shown that SLRPs are involved in the determination of the structural phenotype of collagen fibrils and connective tissue function (Danielson *et al.*, 1997). Decorin-deficient mice have fragile skin characterized by markedly reduced tensile strength and a thinner dermis than normal (Danielson *et al.*, 1997; Zhang *et al.*, 2006). Decorin deficiency also causes variation in collagen diameters *in vivo*, changing the mean and distribution profile of fiber diameters. Collagen alterations are observed throughout the connective tissue in decorin knockouts. Thus, decorin-knockout animals are useful for investigating decorin function in the whole body, though there are technical limitations in revealing the molecular event and mechanism of decorin in collagen fibrogenesis and its detailed assembly process *in vivo*. Despite these reports, much of the relationship between decorin and collagen structure has remained unknown. Especially, the relationship between decorin concentration and collagen fibrogenesis has not been fully determined.

In this study, we investigated the effect of decorin-collagen fibril interaction on collagen fibril assembly and its structure using type I collagen gel, decorin, and siRNA-decorin-transfected (siDT) cells. Collagen fibrils with or without decorin were examined by electron microscopy to determine how they were affected by treatment with decorin. The level of elasticity of collagen gels was measured to evaluate their mechanical strength, and the relationship between their structure and this property was discussed.

Materials and Methods

The procedures used in the experiments are summarized in Figure 1.

Preparation of type I collagen gels

A commercially available kit (Cellmatrix type I-A, Nitta Gelatin, Osaka) of acid-soluble type I collagen gels was used for the reconstruction of collagen fibrils. This kit includes acid-soluble type I collagen, a 10 × minimum essential medium (MEM) and a reconstitution buffer (50 mM NaOH, 250 mM $NaHCO_3$ and 200 mM HEPES). Type I collagen gels were prepared according to the manufacturer's protocols. Briefly, Cellmatrix Type I-A (8 volumes) and 10 × MEM (1 volume) were mixed at 4 ℃ and then the reconstitution buffer (1 volume) was added. Various concentrations of decorin (0.1, 1.0, 5.0, 10 and 25 μg/m*l*; Sigma-Aldrich, St. Louis, MO, USA) were immediately added to the collagen gel mixture, and 1 m*l* of the solution was poured into each well of a 12-well plate. The reconstructed collagen gel mixture was allowed to set over a period of 30 min at 37℃. For the examination of gel contraction, some gels were released from the well wall and left to float in Dulbecco's modified Eagle's medium (DMEM) supplemented with 100 units/m*l* of penicillin and 100 μg/m*l* of streptomycin (Sigma-Aldrich) over a period of 7 days.

siRNA transfection

siRNA-decorin-transfected (siDT) cells were produced by suppressing the gene for decorin in mouse NIH3T3 fibroblasts using RNAi. siRNA was derived from the coding sequence of the mouse decorin gene (Genbank accession number: NM7833). siRNA selection was based on the program B-Bridge Japan (Tokyo). The target sequences and siRNA duplexes for these siRNAs were designated as siRNA (targeted sequence: 5'-AAG AGA GGC UUA UUU GAC UUC-3', sense: 5'-GAG AGG CUU AUU UGA CUU CdTdT-3', antisense: 5'-GAA GUC AAA UAA GCC UCU CdTdT-3').

Experiment design for decorin knockdown in NIH3T3 cells using siRNA

Two days before making the gel and cell mixture, 5×10^4 cells/well were plated in a six-well plate. The following day, one batch of the cells was transfected with GeneEraser (Stratagene, La Jolla, CA, USA) containing 10 nM siRNA in fetal bovine serum-free DMEM. The following day, siRNA-treated or untreated NIH3T3 cells were trypsinized and mixed with the gel solution (cell-gel mixture), and 1 m*l* of the mixture was poured into each well of a 12-well plate (final concentration: 5×10^4 cells/m*l*). Each well wall was coated with 3% poly-2-hydroxyethl methacryate (Sigma-Aldrich) in 95% ethanol to eliminate any adhesion of cells to the growth well surfaces. Some of the cell-gel mixture was poured into glass dishes (1 m*l* of mixture per 17 mm diameter dish) for rheological analyses. After the setting of the cell-gel mixture, the culture medium was added to the gels and changed every 3 days. The cell-gel mixture was sampled on days 15 and 27 after commencing culture in the three-dimensional environment. The cell-gel mixtures were also examined on days 1, 3, and 7 for gel elasticity. After the setting of the cell-gel mixture, treatment with siRNA was performed every 6 days, and some groups were treated with 5.0 or 25 μg/m*l* decorin instead of siRNA on day 18 and 24. Specimens were collected on day 27.

Sample preparation for ultrastructural analysis by scanning electron microscopy and transmission electron microscopy

Collected specimens were prepared for ultrastructural analyses by scanning electron microscopy (SEM) or transmission electron microscopy (TEM). After rinsing with a phosphate buffer, collagen gels were fixed in 3% glutaraldehyde in a 0.1 M phosphate buffer (pH 7.4) for 1 h at 4℃, and then samples were rinsed with distilled water, post-fixed in 1% osmium tetraoxide for 1 h at room temperature, rinsed again with distilled water, and dehydrated in a graded concentration of ethanol. For SEM observation, the specimens were dried by the t-butyl alcohol freeze-drying method (Inoue and Osatake, 1988), mounted on metal stubs, coated with osmium using an osmium coater (Eiko IB3; Ibaraki), and observed

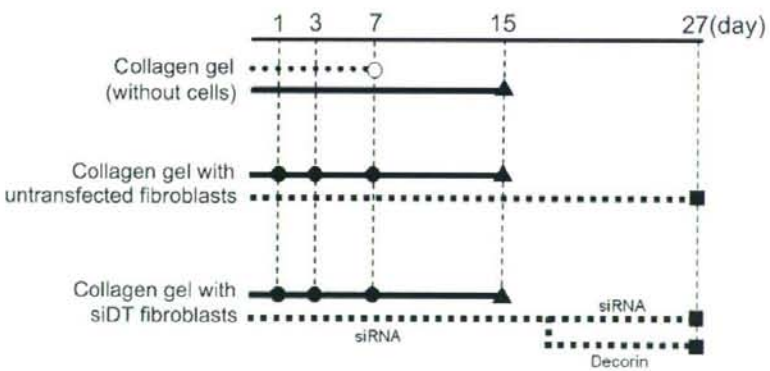

Fig. 1. Summary procedures used in the experimental procedures. Reconstructed collagen gel mixtures with various concentrations of decorin were incubated for 7 days and observed under an electron microscope (○). Specimens of cell-gel mixtures were sampled on days 1, 3, and 7 for measurement of the gel elasticity (●) and for SEM observation of the morphology of collagen fibrils (incubated for 15 days) (▲). SiRNA treatment demonstrated every 6 days and incubated for 27 days. In some specimens, 5.0 or 25 μg/m*l* of decorin was added instead of siRNA from day 18 onwards. These specimens were collected for SEM observation (■).

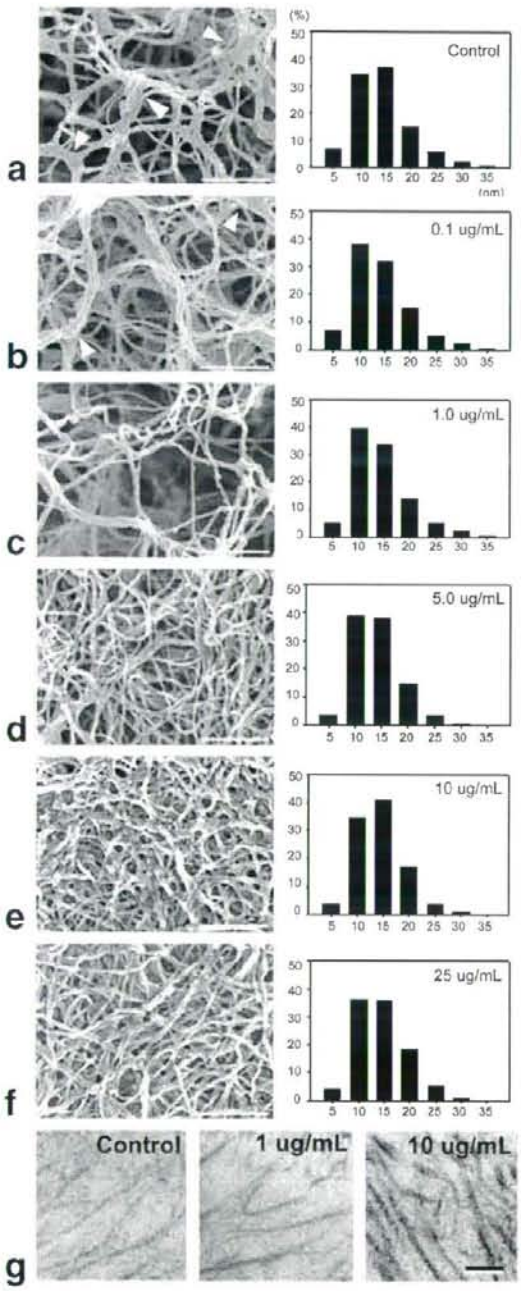

under a scanning electron microscope (JSM-6000F, JEOL, Tokyo) with an accelerating voltage of 3 kV. For TEM observation, the samples were embedded in resin (Quetol 812). Ultra-thin (110 nm in thickness) sections were mounted on a copper grid, stained with 1% uranyl acetate for 8 min and 1% lead citrate for an additional 10 min, and examined by transmission electron microscope (JEM-1200, JEOL) with an accelerating voltage of 80 kV. For measurements of collagen fibril diameter and area of collagen fibrils per unit, 500 fibrils were randomly selected in photographs of each collagen gel. Independent experiments were carried out three times.

Rheological analysis and measurement of gel elasticity

A spherical plunger of 7 mm in diameter was stabbed into the gels at a rate of 0.5 mm/sec using a creep meter (RE-33005, Yamaden, Tokyo). The apparent elasticity of the collagen gels was calculated from the load versus indentation curve obtained using an equation based on Hertz's theory (Lee and Radok, 1960):

$$F = (16\sqrt{R}/3) \times G \times 1.5h,$$

where F is the load (N), R is the radius of the plunger (3.5 mm), G is apparent elasticity (Pa), and h is the indentation (0.7 mm).

Statistical analysis

One-way analysis of variance (ANOVA) followed by Fisher's test using Statview® for Windows, version 5.0, was applied for analyses of the area of collagen fibril per unit, and Student's *t*-test, Microsoft Office Excel 2003 applied rheological analysis. In both results, significant difference was set at $P<0.05$.

Fig. 2. SEM images and histograms of the diameter of collagen fibrils in a collagen fiber network. Collagen fiber network treated with 0 (control, **a**), 0.1 μg/ml (**b**), 1.0 μg/ml (**c**), 5.0 μg/ml (**d**), 10 μg/ml (**e**), and 25 μg/ml (**f**) of decorin. Membranous structures (arrowheads) appear in the fiber network treated with low concentrations (0 and 0.1 μg/ml). Bar=1 μm. **g:** TEM images of collagen fibrils in a collagen fiber network treated with decorin. Bar=100 nm.

Results

Effects of decorin on collagen assembly and fibril diameter

Highly porous collagen fiber networks were formed without decorin (control) or with low concentrations of decorin (0.1 or 1.0 μg/m*l*) (Fig. 2a–c). Membranous structures were often observed in these fiber networks. In contrast, the addition of 5.0 μg/m*l* decorin tightened the mesh network, and similar dense fiber networks were also produced in the samples treated with 10 or 25 μg/m*l* decorin (Fig. 2d–f). Membranous structures were not found in these fiber networks. Furthermore, the gels treated with high concentrations of decorin were not released from the well walls, indicating that the gel did not contract in these samples. The unreleased the gel was still adhered to the well walls at the end of the incubation period (day 7). Between the released gels and unreleased gels, collagen fibril assembly did not appear to differ at any concentration (data not shown).

The average collagen fibril diameter was unchanged regardless of the concentration of decorin, and the median collagen fibril diameter was similar in all specimens. However, the range of collagen fibril diameters in the fiber networks was smaller in the samples treated with a high concentration of decorin than in the samples treated with decorin at a concentration less than 1.0 μg/m*l* (Fig. 2, Table 1). The densities of collagen fibrils (percentage to occupation rate of collagen fibrils in cross section fields) were obtained from TEM micrographs. These values in the fiber networks without decorin (control) and with decorin (0.1, 1.0, 5.0, 10, 25 μg/m*l*) were 9.0 ± 0.3, 10.3 ± 1.3, 9.6 ± 1.0, 16.7 ± 1.0, 16.3 ± 1.5, and 16.5 ± 1.4, respectively. Significantly high densities of collagen fibrils (%) were observed in the samples treated with 5.0 μg/m*l* or more of decorin as compared with the density in controls (Fig. 2, Table 1).

Effect of decorin on collagen fibrils and fiber network elasticity

SEM images showed that collagen fiber networks without fibroblasts were much looser (Fig. 3a) than those cultured with untransfected fibroblasts (Fig. 3b). The networks cultured with untransfected fibroblasts were composed of almost straight fibers with large diameters. On the other hand, collagen fiber networks cultured with siDT fibroblasts were loose and composed of collagen fibers with small diameters (Fig. 3c). The elasticity of collagen fiber networks with untransfected fibroblasts showed no significant difference over the incubation period. In contrast, on days 3 and 7, significantly lower elastic values than that on day 1 were obtained for collagen fiber networks cultured with siDT fibroblasts (Fig. 3d).

Recovery of collagen fibril assembly by addition of decorin after decorin knockdown

Collagen fiber networks cultured with siDT fibroblasts (Fig. 4b) were much looser than networks cultured with untransfected fibroblasts (Fig. 4a). After collagen fiber networks cultured with siDT fibroblasts had been supplemented with 5.0 or 25 μg/m*l* decorin, the structure of the fiber networks changed from loose to dense and became similar to the structure of fiber networks cultured with untransfected fibroblasts (Fig. 4c, d).

Discussion

By morphological and mechanical analyses, we found that decorin significantly influences collagen fibril assembly, diameter, and mechanical strength.

It is thought that decorin binds to the surface of collagen fibrils *via* its core protein and that it regulates collagen fibril morphology (Vogel and Trotter, 1987;

Table 1. Parameter of collagen fibrils

Decorin concentration (μg/m*l*)	0 (control)	0.1	1.0	5.0	10	25
Mean (nm)	11.8 ± 5.37	11.5 ± 5.42	11.5 ± 5.14	11.5 ± 4.44	11.8 ± 4.29	11.7 ± 4.71
Median (nm)	10.8	10.8	10.6	10.8	11.2	11.1
Range (nm)	2.62-35.7	2.62-35.9	3.18-31.9	2.94-28.9	3.17-26.3	3.16-26.8
Density of collagen fibrils in cross section fields (%)	8.95 ± 0.37^a	10.3 ± 1.33^a	9.63 ± 0.97^a	16.3 ± 1.09^b	16.3 ± 1.51^b	16.5 ± 1.15^b

Different letters (*a* and *b*) indicate significant differences ($P<0.05$)

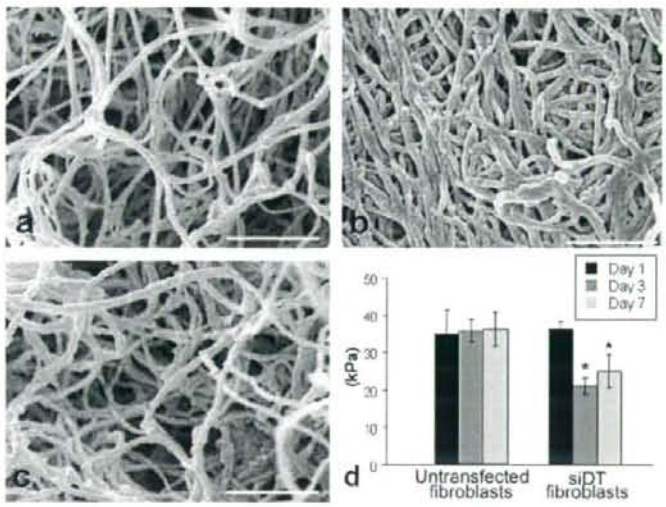

Fig. 3. SEM images of collagen fibrils on day 15 cultured without cells (gel only, **a**), with untransfected fibroblasts (**b**), and with siDT fibroblasts (**c**). Bar=1 μm. Elasticity of the collagen fiber network cultured with untransfected fibroblasts and siDT fibroblasts (**d**). *: Significant difference against the value on day 1 in the same group ($P<0.05$).

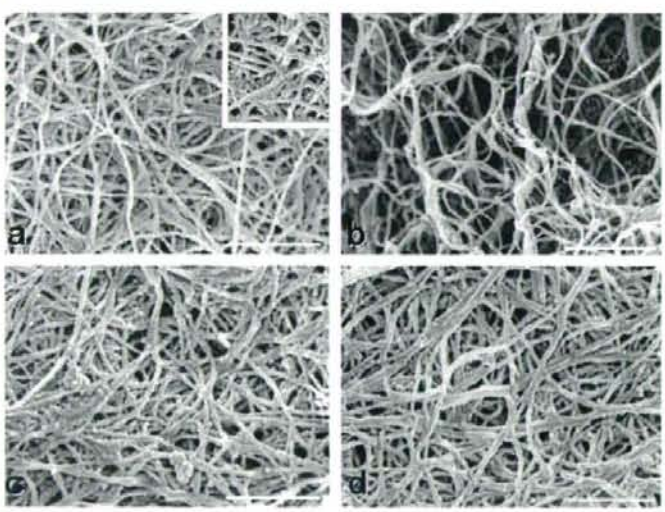

Fig. 4. Effects of decorin on recovery procedure in collagen fibril assembly. All pictures were taken on day 27. Fiber networks cultured with untransfected fibroblasts (**a**) and siDT fibroblasts (**b**) and 5.0 (**c**) or 25 μg/ml decorin (**d**)-treated fiber networks cultured with siDT fibroblasts. Bar=1 μm. **Inset** in **a** is a micrograph of the specimen treated with only a transfection reagent without siRNA.

Bidanset *et al.*, 1992; Scott, 1996, 2001; Raspanti *et al.*, 2002). Decorin also plays a role in the assembly of collagen fibrils, being involved in the determination of fibril diameter (Danielson *et al.*, 1997; Corsi *et al.*, 2002). Our data support results of previous studies and further revealed that an increase in the amount of decorin in the process of collagen assembly results in an increase in density of the collagen fibril network. In addition, membranous structures could be seen in the fiber networks either not treated or treated with very low concentrations of decorin. These findings suggest that decorin is an essential regulatory factor in the process of collagen aggregation.

Danielson *et al.* (1997) demonstrated that decorin-deficient animals exhibited a wider range of collagen fibril diameters than did wild-type specimens. However, our study clarified that decorin has indistinct effects in changing the average diameter of collagen fibrils. Our

study showed that the average diameter of collagen fibrils was not significantly changed regardless of the concentration of decorin. It is generally agreed that decorin is involved in fibril formation because it inhibits an increase in collagen fibril size *in vivo* (Weber *et al.*, 1996; Naeme *et al.*, 2000; Reed and Iozzo, 2002). Our previous studies demonstrated that the density and distribution of collagen fibril diameters in a tendon, which expresses high levels of type I collagen, showed regional differences that were concomitant to the amount of decorin (Watanabe *et al.*, 2005). However, it should be pointed out that various other factors might be involved in the regulation of collagen fibrogenesis *in vivo*, and further studies are needed to identify those factors.

Irregular profiles and abnormal fibril fusion patterns have been observed *in vivo* in decorin-deficient mice. These animals have extremely fragile skin that tears very easily (Danielson *et al.*, 1997; Zhang *et al.*, 2006). In our samples, the elasticity of collagen fiber networks treated with siDT fibroblasts showed significantly lower values. This might be caused by structural fragility due to a lack of decorin. Moreover, the addition of decorin (5.0 or 25 μg/ml) to the samples with siDT fibroblasts allowed collagen to adopt a normal fibril morphology. These results again indicate that decorin is the "architectural" SLRP that maintains collagen fibril configuration and provides strength of structure rheologically.

In the present study, we applied the RNAi method to control the expression of decorin in collagen fiber networks and observed drastic structural changes. Application of RNAi methods to other SLRPs may be useful for understanding the collagen fibrogenesis procedure more precisely. Moreover, suppression of decorin expression using RNAi may possibly serve toward the therapeutic treatment of some connective tissue disorders — such as scar formation — since decorin mRNA and protein are abundantly expressed and localized in scar connective tissue (Napoli *et al.*, 1990; Lee *et al.*, 2004). Thus, injection of decorin mRNA-suppressed cells (*via* decorin gene knockdown) into scar connective tissue may be useful to induce a softening of collagen tissues.

Our study was carried out three-dimensionally by SEM, whereas most previous studies were conducted two-dimensionally by TEM. As Raspanti *et al.* (2007) recently pointed out, TEM has a higher resolution and offers an excellent depiction of detailed collagen structures. We applied TEM to measure the diameter and density of collagen fibers; however, there are limitations in the thickness of the sections (around 100 nm). Under these conditions, the whole structure of the specimens above and below individual sections is difficult to determine unless serial sections are made. By using SEM, we can observe in detail the whole structure of collagen fiber networks, thickness (diameter), and degree of aggregation, fusion, and orientation of collagen fibers.

In conclusion, this *in vitro* study showed that decorin is a key regulatory SLRP in the process of collagen fibril assembly and collagen morphogenesis. However, further, detailed investigation is required to determine the function of each SLRP (biglycan, lumican, and fibromodulin) in the complex process of collagen morphogenesis.

Acknowledgements

The authors are grateful to Dr. Martin Grünert, Institute of Medical Biology, Singapore, for a review of this article, and to Dr. Kunio Nakamura, Department of Rheology, Rakuno Gakuen University, Ebetsu, for advice on measurement of the elasticity of the collagen gel.

References

Bidanset DJ, Guidry C, Rosenberg LC, Choi HU, Timpl R, Hook M: Binding of the proteoglycan decorin to collagen type I. *J Biol Chem* 267: 5250-5256 (1992).

Birk DE, Nurminskaya MV, Zycband EI: Collagen fibrillogenesis in situ: fibril segments undergo post-deponsitional modifications resulting in linear and lateral growth during matrix development. *Dev Dyn* 202: 229-243 (1995).

Birk DE, Hahn RA, Linsenmayer C, Zycband EI: Characterization of collagen fibril segments from chicken embryo cornea, dermis and tendon. *Matrix Biol* 15: 111-118 (1996).

Corsi A, Xu T, Chen XD, Boyde A, Liang J, Mankani M, Sommer B, Iozzo RV, Eichstetter I, Robey PG., Bianco P, Young MF: Phenotypic effects of biglycan deficiency are linked to collagen fibril abnormalities, are synergized by decorin deficiency, and mimic Ehlers-Danlos-like changes in bone and other connective tissues. *J Bone Miner Res* 17: 1180-1189 (2002).

Danielson KG, Baribault H, Holmes DF, Graham H, Kadler KE, Iozzo RV: Targeted disruption of decorin leads to abnormal collagen fibril morphology and skin fragility. *J Cell Biol* 136: 729-743 (1997).

Grinnell F: Fibroblast-collagen-matrix contraction: growth-factor signalling and mechanical loading. *Trends Cell Biol* 10: 362-365 (2000).

Hildebrand A, Romaris M, Rasmussen LM, Heinegard D, Twardzik DR, Border WA, Ruoslahti E: Interaction of the small interstitial proteoglycans biglycan, decorin and fibromodulin with transforming growth factor β. *Biochem J* 302: 527-534 (1994).

Hocking AM, Shinomura T, McQuillan DJ: Leucine-rich repeat glycoproteins of the extracellular matrix. *Matrix Biol* 17:1-19 (1998).

Hosaka Y, Kirisawa R, Mafune N, Takehana K: Downregulation of decorin and transforming growth factor-β1 by decorin gene suppression in tendinocytes. *Connect Tissue Res* 46: 18-26. (2005).

Inoue T, Osatake H: A new drying method of biological specimens for scanning electron microscopy: The t-butyl alcohol freeze-drying method. *Arch Histol Cytol* 51: 53-59 (1988).

Iozzo RV: The biology of the small leucine-rich proteoglycans. Functional network of interactive proteins. *J Biol Chem* 274: 18843-18846 (1999).

Kresse H, Liszio C, Schönherr E, Fisher LW: Critical role of glutamate in a central leucine-rich repeat of decorin for interaction with type I collagen. *J Biol Chem* 18: 18404-18410 (1997).

Kuwaba K, Kobayashi M, Nomura Y, Irie S, Koyama Y: Elongated dermatan sulphate in post-inflammatory healing skin distributes among collagen fibrils separated by enlarged interfibrillar gaps. *Biochem J* 358: 157-163 (2001).

Kuwaba K, Kobayashi M, Nomura Y, Irie S, Koyama Y: Size control of decorin dermatan sulfate during remodeling of collagen fibrils in healing skin. *J Dermatol Sci* 29: 185-194 (2002).

Lee HE, Radok JRM: The contact problem for viscoelastic bodies. *J Appl Mech* 27: 438-44 (1960).

Lee PH, Trowbridge JM, Taylor KR, Morhenn VB, Gallo RL: Dermatan sulfate proteoglycan and glycosaminoglycan synthesis is induced in fibroblasts by transfer to a three-dimensional extracellular environment. *J Biol Chem* 279: 48640-48646 (2004).

Naeme PJ, Kay CJ, McQuillan DJ, Beales MP, Hassell JR: Independent modulation of collagen fibrillogenesis by decorin and lumican. *Cell Mol Life Sci* 57: 859-863 (2000).

Napoli C, Lemieux C, Jorgensen R: Introduction of a chimeric chalcone synthase gene into petunia results in reversible co-suppression of homologous genes in trans. *Plant Cell* 2: 279-289 (1990).

Nareyeck G, Seidler DG, Troyer D, Rauterberg J, Kresse H, Schönherr E: Differential interactions of decorin and decorin mutants with type I and type VI collagens. *Eur J Biochem* 271: 3389-3398 (2004).

Nishimura T, Taneichi A, Wakamatu J, Hattori A: Effect of skeletal muscle decorin on collagen fibrillogenesis in vitro. *Animal Sci J* 74: 399-405 (2003).

Raspanti M, Congiu T, Guizzardi S: Structural aspects of the extracellular matrix of the tendon: an atomic force and scanning electron microscopy study. *Arch Histol Cytol* 65: 37-43 (2002).

Raspanti M, Viola M, Sonaggere M, Tira ME, Tenni R: Collagen fibril structure is affected by collagen concentration and decorin. *Biomacromolecules*. 8: 2087-2091(2007).

Reed CC, Iozzo RV: The role of decorin in collagen fibrillogenesis and skin homeostasis. *Glycoconj J* 19: 249-255 (2002).

Scott JE: Proteodermatan and proteokeratan sulfate (decorin, lumican/fibromodulin) proteins are horseshoe shaped. Implications for their interactions with collagen. *Biochemistry* 35: 8795-8799 (1996).

Scott JE: Structure and function in extracellular matrices depend on interactions between anionic glycosaminoglycans. *Pathol Biol* 49: 284-289 (2001).

Sini P, Denti A, Tira ME, Balduini C: Role of decorin on in vitro fibrillogenesis of type I collagen. *Glycoconj J* 14: 871-874 (1997).

Thieszen SL, Rosenquist TH: Expression of collagens and decorin during aortic arch artery development: implications for matrix pattern formation. *Matrix Biol* 14: 573-582 (1995).

Vogel KG, Trotter JA: The effect of proteoglycans on the morphology of collagen fibrils formed in vitro. *Collagen Relat Res* 7: 105-114 (1987).

Vogel KG, Paulsson M, Heinegard D: Specific inhibition of type I and type II collagen fibrillogenesis by the small proteoglycan of tendon. *Biochem J* 223: 587-597 (1984).

Watanabe T, Hosaka Y, Yamamoto E, Ueda H, Sugawara K, Takahashi H, Takehana K: Control of the collagen fibril diameter in the equine superficial digital flexor tendon in horses by decorin. *J Vet Med Sci* 67: 855-860 (2005).

Watanabe T, Imamura Y, Hosaka Y, Ueda H, Takehana K: Graded arrangement of collagen fibrils in the equine superficial digital flexor tendon. *Connect Tissue Res* 48: 332-337 (2007).

Weber IT, Harrison RW, Iozzo RV: Model structure of decorin and implications for collagen fibrillogenesis. *J Biol Chem* 271: 31767-31770 (1996).

Yamaguchi Y, Mann DM, Ruoslahti E: Negative regulation of transforming growth factor-beta by the proteoglycan decorin. *Nature* 346: 281-284 (1990).

Zhang G, Ezura Y, Chervoneva I, Robinson PS, Beason DP, Carine ET, Soslowsky LJ, Iozzo RV, Birk DE: Decorin regulates assembly of collagen fibrils and acquisition of biomechanical properties during tendon development. *J Cell Biochem* 98: 1436-1449 (2006).

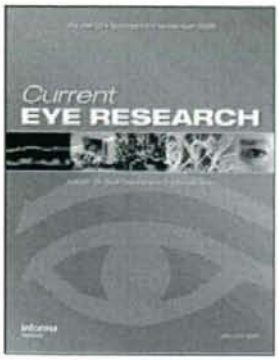

Current Eye Research
Publication details, including instructions for authors and subscription information:
http://www.informaworld.com/smpp/title~content=t713618400

A Preliminary Study of Direct Application of Atelocollagen into a Wound Lesion in the Dog Cornea

Aya Nagayasu [a]; Yoshinao Hosaka [a]; Ayako Yamasaki [c]; Keiko Tsuzuki [c]; Hiromi Ueda [a]; Tomoaki Honda [d]; Kazushige Takehana [a]
[a] Department of Veterinary Anatomy, School of Veterinary Medicine, Rakuno Gakuen University, Ebetsu, Japan [b] Department of Veterinary Anatomy, Faculty of Agriculture, Tottori University, Tottori, Japan [c] Veterinary Teaching Hospital, Rakuno Gakuen University, Ebetsu, Japan [d] Meni-one Co., Ltd., Nagoya, Japan

First Published on: 01 September 2008

To cite this Article Nagayasu, Aya, Hosaka, Yoshinao, Yamasaki, Ayako, Tsuzuki, Keiko, Ueda, Hiromi, Honda, Tomoaki and Takehana, Kazushige(2008)'A Preliminary Study of Direct Application of Atelocollagen into a Wound Lesion in the Dog Cornea',Current Eye Research,33:9,727 — 735
To link to this Article: DOI: 10.1080/02713680802326606
URL: http://dx.doi.org/10.1080/02713680802326606

Current Eye Research, 33:727–735, 2008

ISSN: 0271-3683 print / 1460-2202 online
DOI: 10.1080/02713680802326606

informa
healthcare

A Preliminary Study of Direct Application of Atelocollagen into a Wound Lesion in the Dog Cornea

Aya Nagayasu
Department of Veterinary Anatomy, School of Veterinary Medicine, Rakuno Gakuen University, Ebetsu, Japan

Yoshinao Hosaka
Department of Veterinary Anatomy, School of Veterinary Medicine, Rakuno Gakuen University, Ebetsu, Japan, and Department of Veterinary Anatomy, Faculty of Agriculture, Tottori University, Tottori, Japan

Ayako Yamasaki and Keiko Tsuzuki
Veterinary Teaching Hospital, Rakuno Gakuen University, Ebetsu, Japan

Hiromi Ueda
Department of Veterinary Anatomy, School of Veterinary Medicine, Rakuno Gakuen University, Ebetsu, Japan

Tomoaki Honda
Meni-one Co., Ltd., Nagoya, Japan

Kazushige Takehana
Department of Veterinary Anatomy, School of Veterinary Medicine, Rakuno Gakuen University, Ebetsu, Japan

Received 13 April 2008
Accepted 5 July 2008

Correspondence: Dr. Yoshinao Hosaka, Department of Veterinary Anatomy, Tottori University, 4-101 Koyama-Minami, Tottori 680-8553 Japan. E-mail: y-hosa@muses.tottori-u.ac.jp

ABSTRACT *Purpose:* To evaluate the effectiveness of atelocollagen for canine corneal wound healing. *Materials and Methods:* Atelocollagen was used to fill a transplant bed in the central cornea, which was then covered with a contact lens. The wound healing process was analyzed clinically, morphologically, and biochemically. *Results:* At the early healing stage, both the pupillary zone and details of the iris were observed. The stromal collagen fibrils normalized in a time-dependent manner. Type III collagen in the wound area was detected faintly throughout the experimental period. *Conclusions:* This novel method is advantageous for accelerating wound healing without causing inflammation.

KEYWORDS atelocollagen; collagen fibril; corneal regeneration; dog; keratocyte

INTRODUCTION

Corneal transplantation has been used clinically to treat severe corneal damage. The treatment is selected according to the depth of the corneal wound. For a superficial wound, antibiotic solution and serum are used topically. However, surgical intervention is needed for a deep corneal wound. Surgical procedures most commonly employed include conjunctival grafts and corneal transplantation. Conjunctival grafts accelerate wound healing by supplying blood to the wound area, but scar tissue is formed. In corneal transplantation, there are many problems, including tissue rejection, severe inflammation, scar tissue formation, long repair time, and scarcity of fresh corneal tissue.[1–5]

The canine cornea consists of epithelium, Bowman's layer (rarely present), stroma, Descemet's membrane, and endothelium.[6] The thickness of the cornea is about 0.6 mm, and the corneal stroma is 90–95% of the thickness of the cornea and is composed of keratocytes and an extracellular matrix that consists of collagen fibrils and proteoglycans.[7]

Recently, atelocollagen has been used for treating disorders of the skin and mucous membranes.[8–11] Atelocollagen is a material that is extracted from animal skin, mainly cow and pig skin, and is prepared by pepsin digestion to remove the antigenic telopeptide region from both ends of the collagen molecule. It has a much lower antigenicity than that of normal

collagen with telopeptide. Approximately 95% of the collagen present in this preparation is type I collagen, and the remaining 5% is type III. The purified collagen is mixed with phosphate-buffered saline solution (PBS) and remains in the fluid phase at low temperatures, but on warming to 37°C normal collagen fibrils precipitate, and the collagen solution is transformed into a cohesive, opaque mass. Studies using human subjects[8–11] and experimental animals[12–14] have shown that atelocollagen provides good therapeutic results by promoting cell proliferation and early epithelialization, while causing little rejection and few complications.

For corneal treatment, tissue repair and maintenance of transparency are important. Corneal transparency is maintained by regular spacing of collagen fibrils with remarkable uniform diameter and interfibrillar space.[15] Corneal stroma injury activates keratocytes, which remove the damaged corneal stroma tissue and synthesize collagen fibrils during corneal tissue remodeling.[16] In the normal cornea, as well as other densely connective tissues, such as tendon and ligament, dominant types of collagen are type I and type V. These two types of collagen play a role in the maintenance of corneal transparency. Type III collagen is also present in the cornea, but its ratio is very small. However, in the case of injury, type III collagen is produced to fill the wound area, and the ratio of type III collagen increases. Therefore, type III collagen is understood as "emerging collagen" and is recognized as an index of tissue inflammation.[17–23]

As mentioned above, we hypothesized that atelocollagen treatment of a corneal wound will accelerate corneal healing. To verify this hypothesis, we treated canine corneal wounds with atelocollagen using a novel method and analyzed the wound healing process clinically, morphologically, and biochemically. Overall, we evaluated the effectiveness of the novel method.

MATERIALS AND METHODS

All experiments followed the protocols approved by the Ethics Committee of Rakuno Gakuen University, Japan, and compliance with the NIH Guide for the Care and Use of Laboratory Animals [DHEW (DHHS) Publication No. (NIH) 85-23, revised 1985, Office of Science and Health Reports, DRR/NIH, Bethesda, MD 20205]. Animals were purchased from Kitayama Labes, Nagano, Japan. Animals were housed in light- and temperature-controlled facilities and given food and water *ad libitum*.

Experimental Animals

Four beagles (3 males and 1 female, age 1 year, weighing 9.0–11 kg) with normal ocular and physical health were used in this experiment. Three animals underwent novel treatment on their right eyes. One animal was not subjected to a surgical procedure such as creating a transplant bed and novel treatment, and was used for collecting intact cornea as a control.

For intraoperative pain control, the dogs were premedicated with carprophen (Rimadyl 4 mg/kg, Pfizer Japan, Tokyo, Japan) hypodermically prior to anesthesia and anesthetized with laughing gas, oxygen, and sevoflurane (Sevoflo 2% alveolar concentration (MAC), Dainippon-Sumitomo Pharma, Osaka, Japan). A transplant bed of 0.4 mm in depth and 8 mm in diameter was created by the method of Hanada et al.[24] in the axial cornea of the right eyes with vacuum trephine (Hessburg-Barron vacuum trephine, JEDMED Instrument Company, St. Louis, MO, USA). The transplant bed was filled with 3% atelocollagen (Koken atelocollagen implant, Koken, Tokyo, Japan), which was extracted from calf skin, and then covered with a contact lens for therapy (Meni-one Corneal Bandage One, Meni-one, Nagoya, Japan). A summary of the treatment is shown in Figure 1. Each of the operated animals was given 3% ofloxacin eye drop (Tarivid, Santen, Osaka, Japan) 3 times daily and injected with orbifloxacin (Victas 2.5 mg/kg, Dainippon Sumitomo Pharma, Osaka, Japan) hypodermically once daily until postoperative day 7 (day 7). The dogs were also injected with buprenorphine hydrochloride (Lepetan 0.01 mg/kg, Otsuka Pharmaceutical, Tokyo, Japan) intramuscularly 2 times, after surgery and on day 1 for pain control.

Clinical Examination

Slit lamp examination and direct ophthalmoscopy were performed on the operated eyes to evaluate corneal transparency and visualization of the cornea. Corneal epithelial defects were visualized by topical fluorescein staining methods.[25]

Morphological and Biochemical Analyses

On days 7, 14, and 35, the operated dogs were euthanized using thiopental sodium (Ravonal, Tanabe Seiyaku, Osaka, Japan), and then corneal samples were obtained and divided into two pieces for morphological

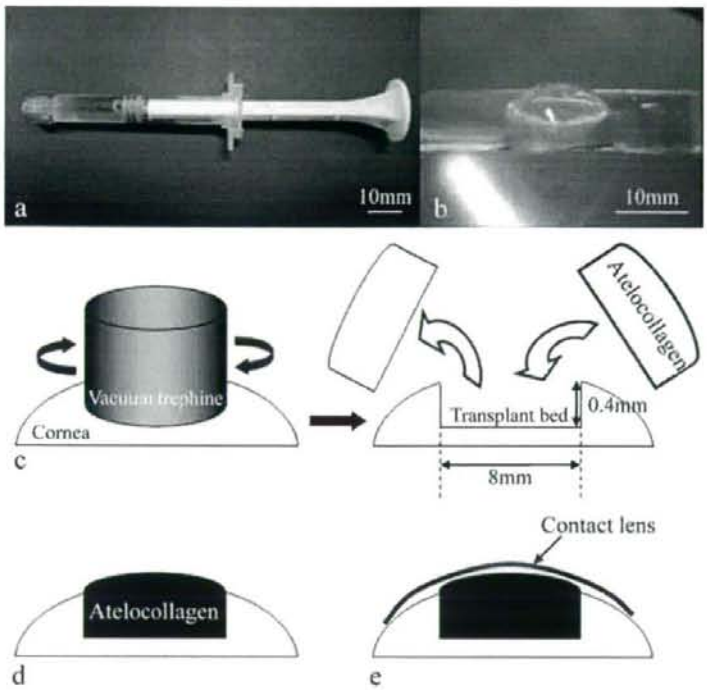

FIGURE 1 Summary of procedure for filling with atelocollagen. Images of 3% atelocollagen (Koken atelocollagen implant; Koken, Tokyo, Japan) (a), and contact lens for therapy (Meni-One Corneal Bandage One; Meni-one, Nagoya, Japan) (b) are shown. After matching the center of a vacuum trephine and the cornea, a transplant bed (diameter: 8 mm, depth: 0.4 mm) is created by turning the vacuum trephine (c). The transplant bed is filled with atelocollagen and then left for about 15 min until the atelocollagen has become opaque (d). The surface of the cornea is covered with a contact lens to prevent atelocollagen from flowing out of the transplant bed (e).

analysis and biochemical analysis. In addition, one sample for light microscopy and three samples for transmission electron microscopy were obtained from the morphological sample. The morphological samples were stored in fixative, and the biochemical samples were stored in a freezer at −80° until use. Intact cornea was also collected and stored in the same way.

Light Microscopy

Corneal samples were fixed in Bouin's solution for 24 hr at room temperature. After dehydration, through an ethanol and xylol series, samples were embedded in paraffin and then cut into 6-μm thick sections, dewaxed, and stained with hematoxylin and eosin. In the experimental corneal wound area, the number of corneal epithelial cell layers and the number of keratocytes per 0.01 mm^2 were counted in 10 areas for each sample. The structures of all of the corneal layers and the corneal epithelium were observed.

Transmission Electron Microscopy (TEM)

Corneal samples (1 × 1 × 1 mm) were fixed in 3.0% glutaraldehyde in 0.1 M phosphate buffer (pH 7.4) for 2 hr at room temperature. Samples were then post-fixed in 1.0% osmium tetroxide in 0.1 M phosphate buffer for 1 hr at room temperature. Thereafter, samples were washed with distilled water, dehydrated in a graded ethanol series, and embedded in Quetol 812 (Nissin EM, Tokyo, Japan). Sections of approximately 60 nm were cut using a Reichert Supernova system (Leica, Milton Keynes, UK) equipped with a diamond knife. Sections were mounted on a copper grid and stained with 0.2% tannic acid with 10% ethanol in water for 15 min. Sections were then stained with 1.0% uranyl acetate for 8 min and 1.0% lead citrate for an additional 10 min and examined by TEM (JEM-1220; JEOL, Tokyo, Japan) at an accelerating voltage of 80 kV. In

the experimental wound area, the basement membrane of the corneal epithelium and arrangement of collagen fibrils were observed, and measurement of collagen fibril parameters was performed for 300 fibrils randomly selected from 10 photographs of each sample. The average collagen fibril diameter and collagen fibril index (CFI) were calculated using the same 10 photographs of each sample.

Collagen Type Analysis

Frozen samples were dissected into blocks of 2 × 2 × 1 mm and subjected to homogenization. To remove non-collagenous components, homogenized samples were suspended in 1 M NaCl/10 mM 2-mercaptoethanol/PBS containing 5 mM EDTA, 0.1 mM phenylmethylsulfonyl fluoride, and 1 mM N-ethylmaleimide for 24 hr at 4°C. The samples were then suspended in 0.5 M acetic acid with pepsin (Worthington Biochemical Corporation, Lakewood, NJ, USA) at 5% of wet weight of tissue for 24 hr at 4°C. Following centrifugation, sodium chloride at a final concentration of 1.7 M was added to the supernatant. Purified collagens were characterized by SDS-polyacrylamide gel electrophoresis (SDS-PAGE) on stacking gel and separating gel with 3.5% and 5.0% of acrylamide, respectively. Type I collagen and type V collagen are heteropolymers $(\alpha 1)_2\alpha 2$, and type III collagen is a homopolymer $(\alpha 1)_3$and has disulfide bonds in the helical region. To permit sufficient separation between the α chains of types I, III, and V collagen, samples were subjected to electrophoresis under delayed reducing conditions according to Sykes' method.[26] Collagen chains that were separated by SDS-PAGE had been stained with Coomassie brilliant blue. Densities of the bands were quantified with NIH imaging software (version 1.61). However, the chains of type V ($\alpha 2$) collagen migrate near the edge of the band of type I ($\alpha 1$), and the ratio of type I ($\alpha 2$) to type V ($\alpha 1$) collagen was therefore calculated.

Statistical Analysis

StatView for Windows (version 5.0) was used to determine means, standard errors, and one-way analysis of variance (ANOVA). Scheffe's test was used to compare differences among the means of number of corneal epithelial cell layers, keratocyte density, collagen fibril diameter, and CFI. Statistical significance was set at the level of $p = 0.05$.

RESULTS

Clinical Examinations

The transplanted atelocollagen became white immediately after surgery, and it was difficult to identify the iris and pupillary zone due to the high opacity of atelocollagen. On day 2, the transparency of transplanted atelocollagen had increased sufficiently to enable identification of the papillary zone. On day 4, details of the iris could be easily observed through the experimental wound area. Transparency of the experimental wound area remained unchanged on days 7 and 14, but was slightly increased on day 35 (Fig. 2).

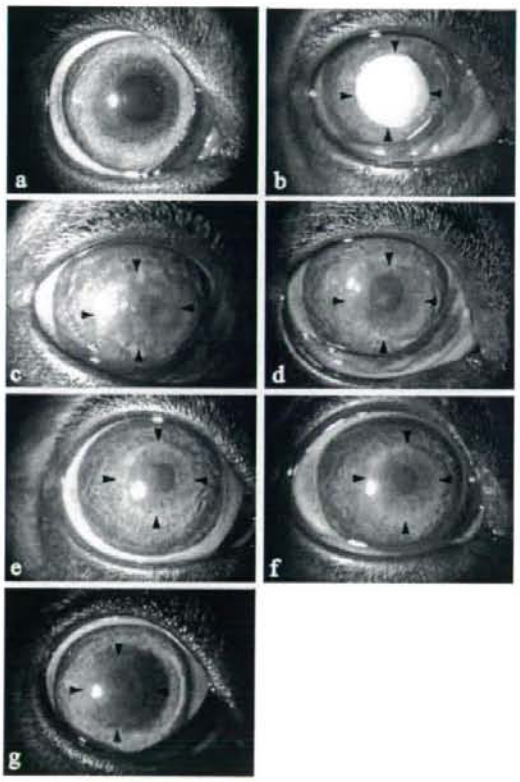

FIGURE 2 Clinical examination of corneal transparency. The condition before the operation is shown (a). The areas enclosed with arrowheads are experimental wound areas. It is difficult to identify the iris and papillary zone due to the high opacity of atelocollagen immediately after surgery (b). On day 2, transparency of the transplanted atelocollagen has increased sufficiently to enable identification of the pupillary zone (c). Details of the iris are observable on days 4, 7 and 14 (d, e and f), and transparency of the experimental wound area has increased slightly on day 35 (g).

FIGURE 3 Detection of corneal epithelial defects by topical fluorescein staining. Defect area of the corneal epithelium is stained extensively on day 1 (a). Stained area on the surface of the cornea has disappeared on day 4 (b). No epithelia are detected in the control (c).

From day 2, vascularization was observed in part of the corneal limbus, and it became to involute on day 7, many winding capillaries were observed in the corneal limbus. After that, the sphere of capillaries got decreased, and no capillaries were observed in this area on day 14. On day 1, extensive topical fluorescein staining showed that the experimental wound area had been unshielded with corneal epithelia. However, the stained area decreased and disappeared by day 4 (Fig. 3), indicating that epithelia covered the surface in the entire wound area.

Morphological Analysis

On day 7, the experimental wound area was already covered with a thick layer of corneal epithelial cells that showed disorderly multiplication. On day 14, the thickness of the layer had decreased, and three cell layers–layers of basal cells, wing cells, and nonkeratinized squamous cells–had formed. On day 35, the corneal epithelium showed normal thickness and composition of cell layers (Fig. 4). The numbers of cells in corneal epithelial layers on days 7, 14, and 35 were 9.4 ± 1.17, 7.4 ± 0.84, and 7.1 ± 0.74, respectively, with the number of cells differing significantly from that in the control cornea only on day 7 ($p < 0.05$).

The basement membrane of the corneal epithelial cells appeared on day 7. On day 14, although the basement membrane had become clearer, it lacked continuity in many areas, with corneal epithelial cells attached to the basement membrane by some hemidesmosomes. On day 35, the basement membrane was uneven but had almost completely formed (Fig. 4).

Keratocyte densities on days 7, 14, and 35 were 25.1 ± 2.88, 22.9 ± 1.17, and 14.3 ± 0.73, respectively, with the numbers of keratocytes on days 7 and 14 differing significantly from those in the control cornea (both $p < 0.05$). TEM observation revealed a large number of keratocytes with large and rounded clear nuclei with indistinct cytoplasm on day 7 compared with the control sample. On day 14, numerous large, spindle-shaped keratocytes with clear nuclei were observed. On day 35, a well-developed, rough endoplasmic reticulum was observed in large cells. Many flat cells were also distributed among the lamellae of collagen fibrils and had long cytoplasmatic processes, like control keratocytes (Fig. 4).

Collagen fibrils were sparse on day 7. Observation of vertical and cross-sections of collagen fibrils showed that the arrangement of collagen fibrils was irregular. On day 14, collagen fibrils were denser, and the arrangement of collagen fibrils was more regular than those on day 7. On day 35, collagen fibril density was high, and the arrangement of collagen fibrils was almost regular, though there was slight disorder. The average sizes of collagen fibrils in the corneal stroma on days 7, 14, and 35 were 24.7 ± 3.30 nm, 25.1 ± 3.83 nm, and 26.1 ± 3.92 nm. The sizes at all timepoints were significantly different to those in the control cornea (all $p < 0.05$). The ratios of collagen fibril area of the corneal stroma on days 7, 14, and 35 were 12.6 ± 4.39%, 17.6 ± 3.29%, and 22.1 ± 7.12%, respectively, with the values on days 7 and 14 being significantly different from on those in the control cornea (both $p < 0.05$). The arrangement of collagen fibrils was irregular on day 7, but became increasingly more regular on days 14 and 35 (Fig. 4). The number of corneal epithelial cell layers, keratocyte density, collagen fibril diameter, and CFI are summarized in Table 1.

Biochemical Analysis

The ratio of types I ($\alpha 2$) to type V ($\alpha 1$) collagen in the control corneal stroma was 83:17. Ratios in the area of corneal injury on days 7, 14, and 35 were 63:37, 75:25 and 55:45, respectively (Table 1). No type III collagen was detected on any postoperative day.

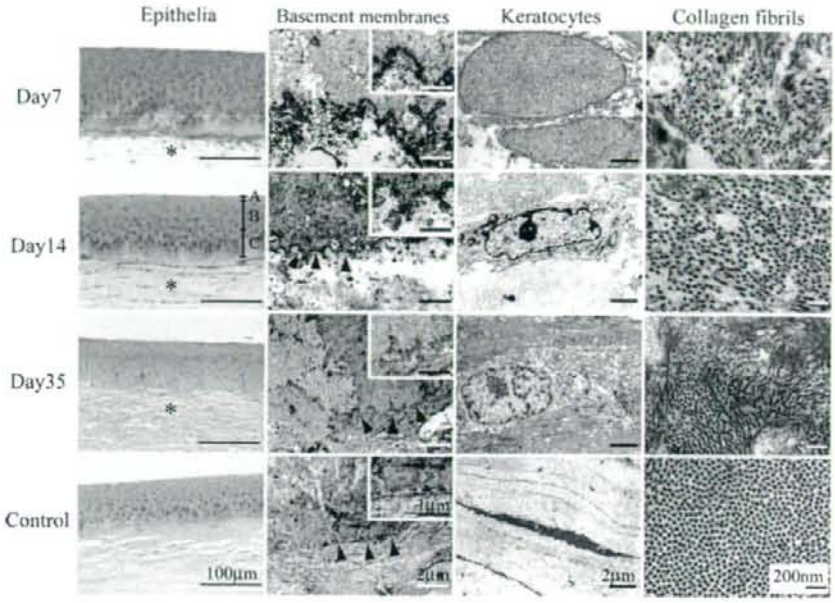

FIGURE 4 Light micrographs and transmission electron micrographs in experimental corneas and control cornea. Experimental wound areas (*) are covered with corneal epithelia. Corneal epithelial cells show disorderly multiplication and hypertrophy on day 7. The corneal epithelium has formed a differentiated layer structure, layers of basal cells (A), wing cells (B) and nonkeratinized squamous cells (C), on day 14 and attained normal thickness on day 35. Basement membranes are shown by arrowheads, and macrographs are shown in the inset at the upper right. Basement membrane is observed in fragments on day 7. Corneal epithelial cells have attached to the basement membrane by some hemidesmosomes on day 14. The basement membrane is uneven but almost completely formed beneath the corneal epithelium on day 35. Most of the keratocytes are large and have rounded clear nuclei with ill-defined cytoplasm on day 7. Numerous keratocytes are large and spindle-shaped with clear nuclei on day 14. Large cytoplasm-rich cells with well-developed rough endoplasmic reticulum are observed on day 35. Collagen fibrils showed an irregular arrangement and sparse distribution on day 7, but the arrangement had become more regular and the density had increased on days 14 and 35.

DISCUSSION

In this experiment, we applied atelocollagen as filler and a scaffold of keratocytes for treating experimental deep corneal wounds. Clinically, some rejection of atelocollagen in the wound region was observed, but it was only mild inflammatory reactions. The injured corneal region was covered with a corneal epithelium on day 4, and corneal transparency gradually recovered.

The canine corneal epithelium has 5 to 7 cell layers, from the base layer to surface, consisting of a single cell layer of basal cells, 2 to 3 layers of wing cells, and 2 to 3 layers of nonkeratinized squamous cells.[7] The healing process of the corneal epithelium can be divided into three overlapping phases: (1) sliding of superficial cells to cover the denuded surface, (2) cell proliferation and differentiation, and (3) reassembly of adhesion structures as basement membrane and

TABLE 1 Number of epithelial cell layers, cell densities, parameters of collagen fibrils, and ratio of collagen type in cornea

	Day 7	Day 14	Day 35	Control
Number of corneal epithelial cell layers	9.4 ± 1.17*	7.4 ± 0.84	7.1 ± 0.74	6.9 ± 0.99
Density of keratocytes (cells/0.01 mm^2)	25.1 ± 2.88*	22.9 ± 1.17*	14.3 ± 0.73	11.8 ± 1.55
Collagen fibril diameter (nm)	24.7 ± 3.30*	25.1 ± 3.83*	26.1 ± 3.92*	28.3 ± 3.49
CFI (%)	8.3 ± 4.51*	14.3 ± 2.65*	26.8 ± 3.13	25.5 ± 2.69
Ratio of type I (α2) to type V (α1) collagen	63:37	75:25	55:45	83:17

Values indicate mean ± SD; *indicates ignificantly different from normal cornea ($p = 0.05$).

hemidesmosomes.[27] On day 7, it was difficult to identify the cellular types and the number of cell layers in the hypertrophic corneal epithelium. However, on day 14, the thickness of the epithelium had decreased compared with that on day 7, and it became possible to identify cell types and the number of cell layers almost as easily as in the control sample. The second healing phase of the corneal epithelium was completed on day 14. The basement membrane and hemidesmosome of corneal epithelia cells were almost restored on day 35. However, some defects of the basement membrane were still present at this timepoint. Therefore, in view of the state of the reassembly of adhesion structure, the healing of the corneal epithelium would be under way in the third phase. This finding was not completely unexpected, however, since it has been reported that complete reconstruction of the basement membrane took 6 to 8 weeks in the process of corneal healing.[28] Therefore, atelocollagen would provide corneal epithelial cells with a suitable environment for epithelial regeneration.

In this experiment, since neovascularization in the wound area after surgery was difficult to detect by clinical examination, migration of inflammatory cells into the wound area was very unlikely. The cells in the corneal stroma would therefore have originated from keratocytes that had migrated from the peripheral wound area. Keratocytes, the dominant cells in the corneal stroma, are thought to have a major function in maintaining homeostasis in the corneal stroma, by the secretion and/or decomposition of extracellular components in the stromal matrix. In the case of injury of the cornea, keratocytes become activated, migrate to the wound site, and begin mitosis.[29,30] If the wound has reached the corneal stroma, keratocyte death resulting from apoptosis occurs around the wound site, and an acellular zone develops. Keratocytes in the region around the acellular zone begin to undergo morphologic change, a process that appears to correspond to their activation. Thereafter, the previously acellular region adjacent to the wound begins to fill with various types of cells indicative of a transitional series between keratocytes and fibroblasts. The cells that have reached the wound edge begin to proliferate, resulting in the formation of a fibroblastic network parallel to the cut surface. The number of cells then decreases.[31,32]

Keratocyte density in the corneal stroma had increased on day 7. Morphological observation revealed that these cells had large and clear nuclei and only a small amount of cytoplasm. These cells may have been highly proliferative keratocytes. The density of cells tended to decrease during the experimental period, and the density of cells was different from that in the control cornea on day 35. Cells with clear nuclei and highly developed rough endoplasmic reticula, which may have been functional enhanced keratocytes, were noted.

Corneal transparency is the result of regular spacing of stromal collagen fibrils with remarkably uniform diameter and interfibrillar space. In the healing process of the corneal stroma, the diameters of collagen fibrils produced by keratocytes are not uniform, and fibrils are present in an irregular arrangement, leading to reduced corneal transparency. The fibrils are then slowly arranged in a consistent direction due to the influence of extracellular matrix components, and the major components, such as collagen and proteoglycans, change to achieve a relatively transparent cornea.[33–35] In the present study, collagen fibril arrangement was irregular, and CFI was lower than that of the control cornea on day 7, but CFI increased thereafter, and the collagen fibril arrangement became regular. The results of this study also support our hypothesis that atelocollagen acted as a scaffold to accelerate keratocyte proliferation, and proliferative keratocytes synthesized collagen fibrils and proteoglycans, leading to reconstruction of the corneal stroma.

In the usual process of wound healing, especially at the early stage of inflammatory reactions, type III collagen synthesis is increased.[20,21,35] However, a number of activated keratocytes were observed in the wound area, and the level of type III collagen was undetectable by biochemical analysis during any healing phase. Although the reason for the lack of type III collagen in the wound area is unclear, inflammatory reaction would have been very slight or would not have occurred in this experiment. We confirmed that the level of type V collagen synthesis during the period of corneal injury repair remained high, as in other tissues such as tendon or ligament. In these connective tissues, tendon and ligament, it has been reported that excessive type V collagen synthesis occurred after injury and that a narrow range of variation in collagen fibril diameter was observed in the healed area.[36–39]

In this study, the ratio of type V collagen increased in the wound region throughout the postoperative period, while the ratio of collagen type I decreased. In the